

Testing the stress shadow hypothesis

Karen R. Felzer and Emily E. Brodsky

Department of Earth and Space Sciences, University of California, Los Angeles, California, USA

Received 29 June 2004; revised 20 January 2005; accepted 17 March 2005; published 4 May 2005.

[1] A fundamental question in earthquake physics is whether aftershocks are predominantly triggered by static stress changes (permanent stress changes associated with fault displacement) or dynamic stresses (temporary stress changes associated with earthquake shaking). Both classes of models provide plausible explanations for earthquake triggering of aftershocks, but only the static stress model predicts stress shadows, or regions in which activity is decreased by a nearby earthquake. To test for whether a main shock has produced a stress shadow, we calculate time ratios, defined as the ratio of the time between the main shock and the first earthquake to follow it and the time between the last earthquake to precede the main shock and the first earthquake to follow it. A single value of the time ratio is calculated for each 10×10 km bin within 1.5 fault lengths of the main shock epicenter. Large values of the time ratio indicate a long wait for the first earthquake to follow the main shock and thus a potential stress shadow, whereas small values indicate the presence of aftershocks. Simulations indicate that the time ratio test should have sufficient sensitivity to detect stress shadows if they are produced in accordance with the rate and state friction model. We evaluate the 1989 M_W 7.0 Loma Prieta, 1992 M_W 7.3 Landers, 1994 M_W 6.7 Northridge, and 1999 M_W 7.1 Hector Mine main shocks. For each main shock, there is a pronounced concentration of small time ratios, indicating the presence of aftershocks, but the number of large time ratios is less than at other times in the catalog. This suggests that stress shadows are not present. By comparing our results to simulations we estimate that we can be at least 98% confident that the Loma Prieta and Landers main shocks did not produce stress shadows and 91% and 84% confident that stress shadows were not generated by the Hector Mine and Northridge main shocks, respectively. We also investigate the long hypothesized existence of a stress shadow following the 1906 San Francisco Bay area earthquake. We find that while Bay Area catalog seismicity rates are lower in the first half of the twentieth century than in the last half of the nineteenth, this seismicity contrast is also true outside of the Bay Area, in regions not expected to contain a stress shadow. This suggests that the rate change is due to a more system wide effect, such as errors in the historical catalog or the decay of aftershocks of the larger 1857 Fort Tejon earthquake.

Citation: Felzer, K. R., and E. E. Brodsky (2005), Testing the stress shadow hypothesis, *J. Geophys. Res.*, 110, B05S09, doi:10.1029/2004JB003277.

1. Introduction

[2] After the San Francisco earthquake of 1906 one pressing question was when the next big earthquake would occur. While G. Ashley of the U.S. Geological Survey stated that geological evidence suggested that earthquakes of equal or larger size were “liable to occur at any time in the future” [*Geschwind*, 2001, p. 37], most seismologists, working under an idea that would later formally be known as the seismic gap hypothesis [*Davies et al.*, 1981; *Kagan and Jackson*, 1991], assumed that some recovery time to replace the stress released by the earthquake would be required and predicted a sustained period of quiescence. Omori estimated that the great earthquake would not repeat

itself for at least 30 years [*Omori*, 1907]; *Reid* [1910] predicted that the next large earthquake on the San Andreas fault would not occur for another century [*Geschwind*, 2001]. *Willis* [1924] looked beyond the main shock fault and predicted that seismicity over the entire Bay Area would be subdued for at least 30 years.

[3] Willis’ prediction of region-wide quiescence after the 1906 earthquake came from the hypothesis that most of the stress had been released not just from the fault but from the entire system by the 1906 rupture. It is now known that the static stress changes experienced by most faults as a result of nearby earthquakes, on the order of a bar to tenths of bars, are actually quite small in comparison to earthquake stress drop. Yet it is widely hypothesized that these small static stress changes are the primary agents in the triggering of aftershocks when the stress changes are positive, and the stress shadow model predicts that these

static stress changes are likewise capable of decreasing seismicity rates where they are negative [Simpson and Reasenber, 1994].

[4] Alternatively, it has been argued that the small static stress changes are insignificant agents of earthquake interaction in comparison to the much larger, albeit temporary, dynamic stresses associated with earthquake shaking. The idea that dynamic stresses can trigger earthquakes has been proven by the existence of triggered earthquakes at distances too far to have been affected by static stress changes [e.g., Hill *et al.*, 1993]. For nearby or “traditional” aftershocks, however, it is controversial whether static or dynamic stress changes are more important. A number of authors have demonstrated that aftershocks are somewhat more likely to occur where static stresses are increased by a main shock [King *et al.*, 1994; Hardebeck *et al.*, 1998; Toda *et al.*, 1998], but it has also been found that the radiation pattern of dynamic stresses can explain aftershock locations at least as well as static stress change patterns [Kilb *et al.*, 2002]. Asymmetry in aftershock locations following the direction of main shock propagation suggests dynamic triggering [Gomberg *et al.*, 2003]; static stress changes should not be able to produce such asymmetrical effects. However, not every aftershock sequence shows such asymmetry.

[5] One of the significant differences between static and dynamic stresses is the production of stress shadows [Marone, 2000; Stein, 2003]. Static stress changes are described by a single stress tensor, while dynamic stress changes, which are oscillatory, produce forcing in opposite directions. Before the imposition of stress changes a given fault will have deviatoric shear stresses and a corresponding preferred slip direction that are a function of the background tectonic stresses. If static stress changes are added that are in opposition to the background stresses the rupture of the fault will be delayed. This will produce a stress shadow. The only circumstances under which we do not expect to see such a shadow are if the imposed static stress changes agree everywhere with the existing background stress direction, a scenario that is highly unlikely, or if static stress change does not significantly affect earthquake timing. Because stress shadows are one observable produced by static but not dynamic triggering, the clear observation of stress shadows on a regular basis would provide evidence in favor of the dominance of static stress triggering.

[6] In this paper we define a stress shadow specifically as the phenomena which is expected to occur if all or the vast majority of aftershocks are triggered by static stress changes mediated by rate and state friction, as expressed in the model by Dieterich [1994]. These shadows commence immediately at the time of the main shock and then slowly recover. First we will discuss some previous methods that have been used to look for stress shadows and why these methods might be problematic. We will then use our new time ratio method to look for stress shadows following the 1989 M_W 7.0 Loma Prieta, 1992 M_W 7.3 Landers, 1994 M_W 6.7 Northridge, and 1999 M_W 7.1 Hector Mine earthquakes. Finally, we investigate the 1906 San Francisco earthquake. We find that although seismicity in the San Francisco Bay Area was quieter, on average, over the 50 year period after 1906, this quiescence started some time after the main

shock and extended southward along the San Andreas fault system to areas where a stress shadow from 1906 is not expected. This suggests an alternate cause for the seismicity rate decrease observation.

2. Some Previously Proposed Stress Shadow Tests

[7] Potential stress shadows have been proposed after a number of recent California earthquakes, including the 1989 M_W 7.0 Loma Prieta earthquake [Reasenber and Simpson, 1992; Parsons *et al.*, 1999; Stein, 1999], and the 1992 M_W 7.3 Landers earthquake [Wyss and Wiemer, 2000]. However, it has been shown by Marsan [2003] that many of the methods used in stress shadow studies are questionable. In particular, Marsan [2003] pointed out problems resulting from assumptions that the seismicity rate is stationary and Gaussian. In reality, most earthquakes are aftershocks, and the earthquake rate in aftershock sequences continuously decays with time. It is extremely difficult to adequately account for the constant decay of numerous scattered aftershock sequences when looking for stress shadows.

[8] The simplest method that is commonly used to correct for decaying aftershock sequences is to try to remove aftershocks, or decluster the catalog, before inspecting for rate changes. Declustering often consists of removal of earthquakes that occur in somewhat arbitrary space and time windows. The declustered catalog is then assumed to be Poissonian, and a test is done to see if there are significant differences in long-term average seismicity rates measured before and after the main shock. This method has been used to claim evidence for stress shadows following the Loma Prieta earthquake [Reasenber and Simpson, 1992] and Landers earthquake [Wyss and Wiemer, 2000], among others. The first problem is that while these declustering algorithms are an excellent way of identifying some aftershocks, they cannot identify all of them. It was demonstrated by Reasenber and Simpson [1997], for the Loma Prieta earthquake, that the failure to remove all aftershocks will produce some spurious signals when searching for stress shadows. We investigate the region around the 1989 Loma Prieta earthquake, declustering the catalog using an algorithm based on the work by Reasenber [1985]. We then compare seismicity rates before and after the Loma Prieta earthquake, and before and after a date on which no large earthquake happened, a year before the Loma Prieta earthquake (Figure 1). We find significant seismicity rate decreases in the declustered catalog in both cases, with a larger area of decrease occurring around the date a year before Loma Prieta, when no stress shadow is predicted. This indicates that it might be hard to verify stress shadows seen with this method.

[9] Other researchers have tried to model aftershocks rather than remove them [Ogata *et al.*, 2003; Woessner *et al.*, 2004]. In particular, a potential (but much smaller than expected) stress shadow of the Loma Prieta was found with this method by Marsan [2003]. Using this technique a stress shadow is indicated if the aftershock sequences becomes less active than predicted. To predict the activity of an aftershock sequence, parameters for the modified Omori law, which describes aftershock decay, are fit to the portion of the aftershock sequence occurring before some hypothesized stress-shadow-inducing main shock. The problem is

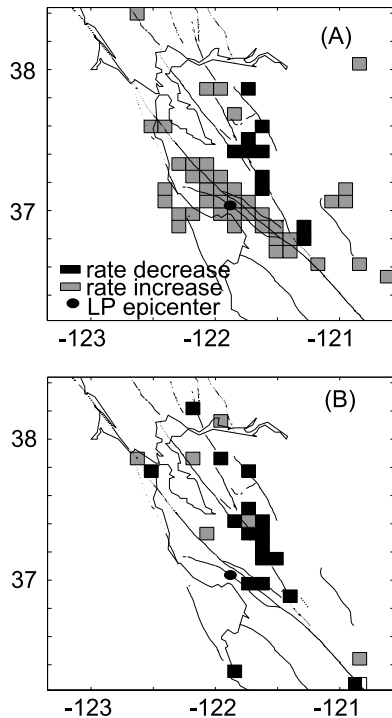


Figure 1. (a) Using a declustered catalog, we compare seismicity rates in the year after Loma Prieta to the average seismicity rate over the preceding 6 years. Positive rate changes are in gray, negative are in black. Rate changes plotted are significant at the 98% confidence level, assuming that the declustered catalog is Poissonian. (b) Comparison of seismicity rates in the year before Loma Prieta compared to the rates in the preceding 6 years. Note that there is actually a larger area covered by significant negative rate changes in this case, when nothing occurred to create a stress shadow. Each bin is 10×10 km.

that projections of this sort have a systematic tendency to overpredict the latter part of the aftershock sequence. This is because the combining of a large number of secondary aftershock sequences in the real data causes the global modified Omori law p value (the exponent of the inverse power law relationship) to increase with time [Sornette and Sornette, 1999; Helmstetter and Sornette, 2002; Felzer et al., 2003]. An increasing p value is equivalent to an increasing decay rate. The p value also often further increases with time because of incomplete recording of the earliest aftershocks. Because of these problems we find, in our own trials, that we observe “stress shadows” even when none are expected to exist. For the aftershock sequence of the 1987 M_w 5.7 Palm Springs earthquake, for example, we find that the sequence begins dipping below the projection of the best fitting modified Omori law shortly beyond whichever point in time we fit the law to (Figure 2).

[10] An alternative method for dealing with interfering aftershock sequences is to note that aftershock decay is generally a gradual process. Thus instead of looking for long time-averaged decreases in the seismicity rate several authors have looked for sudden decreases in the seismicity rate at the time of a large main shock. Among others, this

technique has been applied to the Loma Prieta earthquake [Stein, 1999], the Landers earthquake [Wyss and Wiemer, 2000] and several earthquakes in Kagoshima, Japan [Toda and Stein, 2003]. Authors that use this technique generally claim stress shadow existence if any single region within the predicted stress shadow, of any size, demonstrates this sudden rate decrease. However, sudden rate decreases can happen in a limited region without the presence of an actual shadow in at least two ways. The first potential cause of a sudden rate change is temporal changes in the completeness magnitude threshold. In the immediate aftermath of any large main shock the network will be overwhelmed by activity and the magnitude threshold will increase; several days or a week thereafter the threshold may turn around and dip below its normal level as temporary stations are deployed and analysts pay extra attention to the data. When a foreshock precedes a main shock with some significant time delay, as occurred in the case of the Loma Prieta earthquake, the magnitude threshold may be particularly unstable, rising and then falling before the main shock (and thus artificially increasing premain shock seismicity rates), and then rising and falling again.

[11] The second reason for a sudden regional reduction in the seismicity rate is the simultaneous decaying of several local aftershock sequences that started at various times before the main shock and are in decay after it. Combining these sequences creates the appearance of a continuously elevated activity rate before the main shock and a lower rate afterward (Figure 3). Since small aftershock sequences are quite common at all times and places, subregions containing rate changes caused by this effect can usually be found centered around any random point in time.

[12] In the face of the numerous difficulties that ongoing local aftershock decay causes for many existing stress shadow tests we have designed a new method to test for stress shadows, the time ratio test, which is described below. This method reduces the influence of ongoing aftershock decay by only using the times of the earthquakes occurring

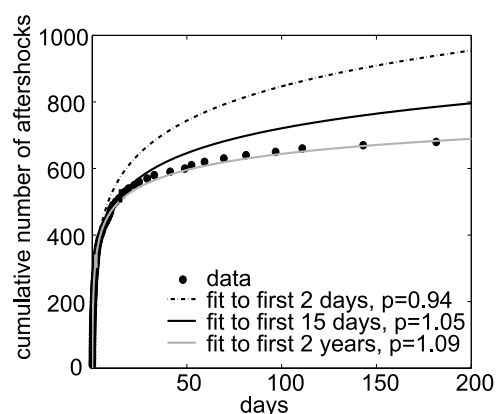


Figure 2. We plot of earthquakes occurring after the 1987 M 5.7 Palm Springs earthquake with the modified Omori laws that best fit the first 2 days (dot-dashed black line), the first 15 days (black line) and first 2 years (gray line) of the sequence, respectively. The data consist of $M > 2.0$ aftershocks.

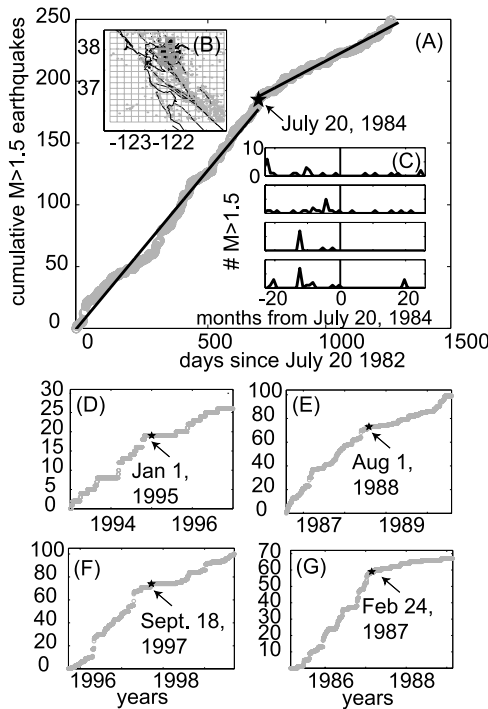


Figure 3. To test whether sudden changes in seismicity rate may be seen in a selected region at any time, we look in the San Francisco Bay Area on the arbitrary date of 20 July 1984 (no large earthquake on this date). We identify boundaries of a continuous subregion by looking for a region with a lower earthquake rate after 20 July 1984 than before. (a) Cumulative earthquake time series in our subregion. A sudden rate decrease is seen on 20 July 1984. (b) Map of the Bay Area, with earthquakes in the selected subregion plotted in black. Boxes surround small clusters in the subregion. (c) Separate time histories for the earthquakes within four of the boxes. It can be seen that the sudden 20 July decrease is caused by a combination of particular aftershock sequences. (d)–(g) Demonstration of the universality of this effect for four additional dates with a random number generator chosen.

immediately before and immediately after the main shock in different spatial bins.

3. Time Ratio Test

3.1. Defining the Time Ratio

[13] To test for stress shadows, we set as the null hypothesis that stress shadows do not exist and then see if we can find regional seismicity rate decreases initiated at the time of the main shock that are strong enough to disprove this hypothesis. To do this test, we need a method that is sensitive to seismicity rate changes initiated at the time of the main shock but insensitive to ongoing rate changes, such as decaying aftershock sequences. Ongoing rate changes are composed of systematic trends in earthquake interevent times (e.g., interevent times becoming progressively shorter or longer). In order to see these systematic trends at least two interevent times are needed. Isolation from ongoing rate changes can thus be achieved if we study

only a single interevent time, framed by just two earthquakes. At the same time, the times of just two earthquakes, if there is a main shock in between them, is sufficient to provide information about whether the main shock changed the seismicity rate. To show this, we first assume that we have an infinitely long catalog (finite catalog effects will be discussed later) and assume that if the main shock had no effect, the time interval between the two earthquakes would be ΔT_0 . We also assume that the timing of the first earthquake of the pair (occurring before the main shock) and the time of the main shock are independent of each other. Because of this independence, the time gap between this first earthquake and the main shock, which we will call Δt_1 , should be uniformly distributed between 0 and ΔT_0 . We then define Δt_2 as the time lag between the main shock and the second earthquake (variables are illustrated in Figure 4), and define the time ratio, R , as follows:

$$R = \frac{\Delta t_2}{\Delta T} \quad (1)$$

where ΔT is the new earthquake interevent time, after the main shock has had the opportunity to influence the timing of the second earthquake. If the main shock fails to change the timing of the second earthquake then $\Delta T = \Delta T_0$ and $\Delta t_2 = (\Delta T - \Delta t_1) = (\Delta T_0 - \Delta t_1)$ will be uniformly distributed between 0 and ΔT . Thus in this case values of the time ratio will be uniformly distributed between 0 and 1.

[14] If the main shock influences the timing of the second earthquake then $\Delta T \neq \Delta T_0$ and Δt_2 will no longer be uniformly distributed between 0 and ΔT . If the earthquake rate is sped up by the main shock Δt_2 will tend to be small in comparison to ΔT , producing values of the time ratio near 0. If the main shock slows earthquakes down then Δt_2 will tend to be long in comparison to ΔT and there will be a concentration of time ratio values near one.

[15] According to the static stress change earthquake triggering model, main shocks are expected to produce rate increases, or aftershocks, in some areas, and slow downs, or stress shadows, in others. Thus we break the region within 1.5 fault lengths of each main shock down into 10×10 km spatial bins and calculate a separate value of the time ratio for each bin. We use 10 km as our length scale because we find that 10×10 km bins are the smallest bins for which stress shadows are reliably visible in simulations (described

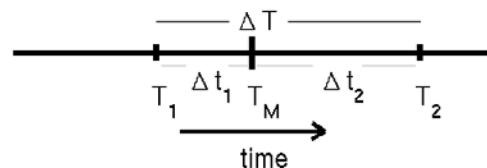


Figure 4. The diagram illustrates variables used to calculate the time ratio. The diagram is for earthquakes in a single 10×10 km bin. Time increases to the right, and each vertical mark indicates the time of one earthquake. T_M is the time of the main shock, T_1 and T_2 are the times of the earthquakes before and after the main shock, respectively, Δt_2 is the time between the main shock and the first earthquake to follow it, and ΔT is the time between the last earthquake to precede the main shock and the first to follow it.

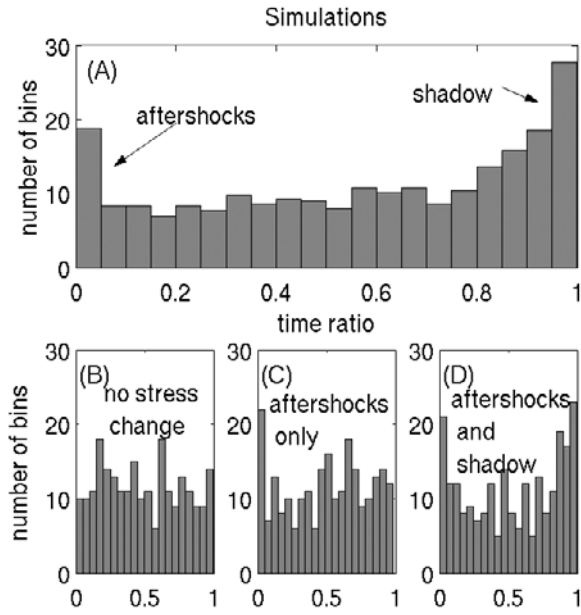


Figure 5. Using simulations, we plot examples of what types of time ratio distributions we would expect to see with and without aftershocks and stress shadows. The simulations are based on the stress change map of the Landers earthquake and use randomly placed earthquakes with a rate set twice as high as the real premain shock catalog in order to demonstrate behavior when the seismicity rate is high in comparison with catalog length, equivalent to the case of having seismicity at any rate in an infinite catalog. Description of the simulation method is given in section 4.2. (a) Average of 10 simulations with stress increases and decreases imposed on the data. Peaks near zero and one indicate the presence of aftershocks and a stress shadow, respectively. (b) One simulation with no stress changes imposed. (c) One simulation, positive stress changes only. (d) One simulation, stress increases and decreases.

below). In a probability density function of the time ratio values we expect a peak near zero if there are aftershocks and a corresponding peak near one if there is a stress shadow (Figure 5).

[16] In order to evaluate whether a stress shadow is indicated by any particular time ratio distribution we need a way to measure quantitatively how large of a peak of time ratio values near 1 a distribution has. We do so by using a metric that we will call the shadow factor, S . The shadow factor is measured from the second half of the time ratio distribution, with time ratios between 0.5 and 1, so that it is minimally influenced by the aftershocks that dominate the first half of the range. We estimate the probability density function (PDF) of the time ratio distribution between 0.5 and 1 with a 25 bin histogram. We then take the range of the data, the maximum difference in height between any two histogram bins, and normalize this value by the total number of spatial bins that have time ratios between 0.5 and 1. If we express the heights of the histogram bins as $H(R)$ we have that

$$S = \frac{\max(H(R)) - \min(H(R))}{\sum_{0.5}^1 H(R)} \quad (2)$$

where for the whole equation we only consider values of R between 0.5 and 1. If a stress shadow causes the time ratio distribution to steeply increase between 0.5 and 1 then there will be a large range, and a large shadow factor. Random variations between 0.5 and 1 will be nonsystematic and therefore have a smaller range.

[17] Up to now we have assumed that our earthquake catalog is infinitely long. Our results will be the same for a finite catalog as long as in all bins $\Delta T_0 < (T_E - T_M)$ and $\Delta T_0 < (T_M - T_S)$, where T_S is the starting time of the catalog, T_E is the ending time of the catalog, and T_M is the time of the main shock. Under these conditions the last earthquake preceding the main shock and the first earthquake following it will always be visible in the catalog. If ΔT_0 is so large that both earthquakes cannot be seen at all times, then we will only measure a limited range of time ratios. In particular, time ratio values smaller than $L_1 = (\Delta T_0 - (T_M - T_S))/\Delta T_0$ or larger than $L_2 = (T_E - T_M)/\Delta T_0$ correspond to earthquakes being before the beginning or after the end of the catalog, respectively, and will not be measured. Between L_1 and L_2 , the time ratio distribution will be uniform. Because different bins have different values of ΔT_0 , however, different bins have different values of L_1 and L_2 , and combining uniform distributions with different endpoints produces a nonuniform distribution peaked near the middle where all of the distributions overlap.

[18] At least the above applies if we only measure a value of the time ratio when at least one earthquake before and at least one earthquake after the main shock are present in the catalog. In fact we cannot afford to neglect all bins that are missing an earthquake. Simulations (described below) show that many of the bins that experience significant stress shadowing have no catalog earthquakes after the main shock, and that leaving these bins out of the analysis makes it very difficult to see the stress shadow. Thus we estimate a time ratio when the earthquake after the main shock is missing. We do this by first calculating the minimum possible time ratio for each bin,

$$R_{\min} = \frac{T_E - T_M}{\Delta t_1 + (T_E - T_M)} \quad (3)$$

where T_M is the time of the main shock, T_E is the end time of the catalog, and Δt_1 is the time between the main shock and the last earthquake to precede it. Then we assign a random time ratio, with uniform probability, between R_{\min} and 1.0.

[19] When we estimate the time ratio in this manner we introduce additional nonuniformities to the time ratio distribution. This is because when the first earthquake after the main shock is off the end of the catalog each value of Δt_1 no longer corresponds to a single value of the time ratio for a given ΔT_0 but rather to a uniform distribution of time ratios between R_{\min} and 1.0. The probability of getting a given value of the time ratio, R , is then given by

$$P(R) = \int_{(T_E - T_M)(\frac{1-R}{R})}^{T_M - T_S} P(R|\Delta t_1)P(\Delta t_1)d\Delta t_1, \quad (4)$$

where $P(R|\Delta t_1) = 1/(1 - R_{\min})$, because R is chosen from a uniform distribution between R_{\min} and 1.0, and $P(\Delta t_1) =$

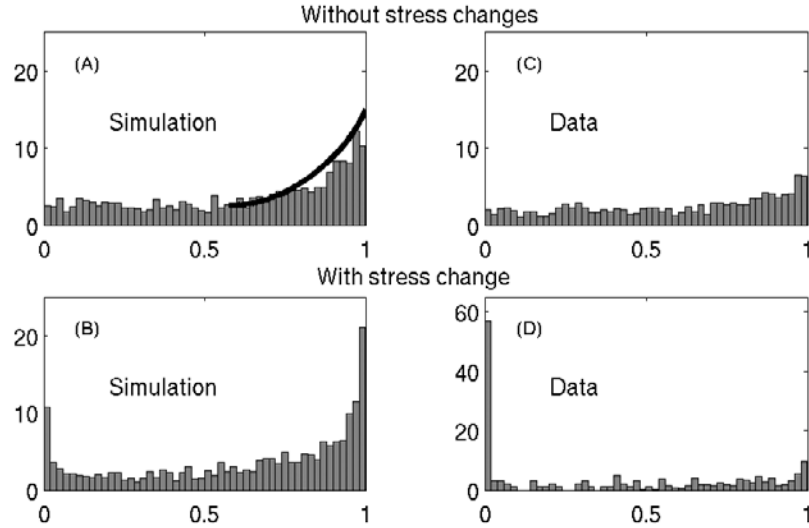


Figure 6. Each plot represents the average of 10 time ratio distributions calculated for the region around the Landers earthquake, with and without main shock-induced stress changes imposed. Simulation results are given in Figures 6a and 6b and calculations for real data are given in Figures 6c and 6d. (a) Simulation is done without any imposed stress changes. The second half of the distribution is plotted with the predicted time ratio distribution from equation (4). (b) Simulation has stress increases and decreases imposed. Simulations are done with the data-based method using the stress change map as calculated (not randomized) and using the best fit seismicity rates (see text). (c) Average time ratios are from 10 control catalogs centered around times before the Landers earthquake (when no large shadows are expected). (d) Time ratio distribution is centered around the time of the Landers main shock. Note the different y axis for this plot.

$1/(T_M - T_S)$ since Δt_1 covers a uniform distribution between 0 and $T_M - T_S$. The upper limit of integration is the largest possible value of Δt_1 for any value of R . The lower limit of Δt_1 is the smallest that Δt_1 can be for each value of R , under the constraint that the first earthquake after the main shock has to be after the end of the catalog (e.g., $\Delta t_2 > (T_E - T_M)$). The limit can be derived by combining this constraint on Δt_2 and equation (1), noting that $\Delta T = \Delta t_1 + \Delta t_2$.

[20] Solving equation (4) yields a probability density function of R that increases logarithmically with increasing R . Another way to see that the probability distribution will behave this way is to note that for all of the possible values of Δt_1 the corresponding distribution of R includes values near 1.0, but only a few distributions of R include values near the smaller end of the range. Adding these distributions together causes the probability density function of the time ratio to increase with increasing R . The peak near 1.0 produced by this effect is significantly smaller than the peak produced by a stress shadow on the same data set, except in the cases where seismicity rates are so low that few bins will have earthquakes after the main shock with or without a shadow. For instance, in simulations of the Landers earthquake there is a larger peak near 1.0 in the time ratio distribution when a stress shadow is present than when it is absent (Figures 6a and 6b). The solution of equation (4) is also plotted in Figure 6b.

[21] In addition to large values of ΔT_0 , nonuniformities in the time ratio distribution may be produced if different spatial bins are correlated with each other. Because the main shock is fixed in time, a random distribution of Δt_1 , important for a random distribution of time ratios, can only be obtained if the earthquakes preceding the main shock in

each bin are randomly distributed in time with respect to each other. Because the bins are 10×10 km in size, larger than the dimensions of most small aftershock sequences, we expect that this random distribution will generally prevail unless there is a large aftershock sequence initiated by another earthquake close in time to the target main shock.

[22] The biases in the time ratio distribution mean that we cannot evaluate the significance of the shadow factor by comparing it statistically to a uniform distribution. Instead we need to compare the shadow factor that we measure at the time of the main shock to a distribution of shadow factors measured from “control” earthquake catalogs that do not contain large main shocks, and hence no large shadows. Our control catalogs consist of 100 randomly selected, internally sequential, subcatalogs from the premain shock time period (e.g., from 1 January 1984, the point from which southern California catalog magnitudes are reasonably self-consistent, to the time of the main shock.) An effective main shock date is assigned to each of these subcatalogs such that there is the same ratio of catalog time before and after this date as for the real main shock. We calculate the mean and standard deviation of the shadow factors calculated from the control catalogs and use these to define the normalized shadow factor, \hat{S} , as follows:

$$\hat{S} = \frac{S - \bar{S}_C}{\sigma(S_C)} \quad (5)$$

where S is the shadow factor measured at the time of the main shock, \bar{S}_C is the mean of the shadow factors in the control catalogs, and $\sigma(S_C)$ is the standard deviation of the shadow factors in the control catalogs.

[23] A standard deviation is assigned to the normalized shadow factor by doing 100 calculations of the shadow factor at the time of the main shock with different random selections for the time ratios for bins that do not have earthquakes after the main shock. To constrain error, we also measure the shadow factor at the time of the main shock both with the whole catalog and with a subcatalog that is the same length as the control subcatalogs.

[24] Our calculations are done with $M \geq 2.3$ earthquakes for the Landers, Loma Prieta, and Hector Mine earthquakes. We find $M \geq 2.3$ to be a fairly conservative completeness threshold for the data by comparing mean catalog magnitudes with the mean expected in a perfect Gutenberg-Richter distribution [Ishimoto and Iida, 1939; Gutenberg and Richter, 1944] with a b value of 1.0. For the Northridge earthquake we go down to $M \geq 2.0$; this is justified by the better station coverage in the Los Angeles area and made necessary by the sparse premain shock seismicity. For the Landers earthquake we use the catalog from 1 January 1984 until the occurrence of the Hector Mine main shock in October 1999 where we stop to avoid interference between the two earthquakes. For all of the other earthquakes we use Advanced National Seismic System (ANSS) catalog data through the end of 2003.

[25] If the normalized shadow factor is large (>2 , as discussed below), indicating that the wait time for the first earthquake to occur after the main shock is significantly long in a number of spatial bins, then the null hypothesis can be rejected at high confidence. In this case stress shadows exist, and we are done with our exercise. If the null hypothesis is not rejected, however, as is the case for our data (more details below) there remains the possibility that a stress shadow still exists but is simply below the sensitivity level of our test. To investigate this possibility (also known as a type II error), we create simulated catalogs with imposed stress shadows to see the range of normalized shadow factors produced when we know a stress shadow is present. These simulations are described below.

3.2. Simulations

[26] We produce simulated earthquake catalogs with and without static stress changes imposed on them to test the sensitivity of the normalized shadow factor. The simulations are run by first calculating static Coulomb stress changes produced by the main shock, assuming a uniform elastic half-space, and then applying the rate and state friction equations [Dieterich, 1994] to translate those stress changes into earthquake timing changes.

[27] We calculate the static stress change maps using the program Coulomb 2.6 [Toda and Stein, 2002] and using a background stress of 100 bars. For the fault and slip parameters of the Landers earthquake we use the file provided with the Coulomb program, which is based on the work by Wald and Heaton [1994]. Slip for the Loma Prieta earthquake is approximated as a single plane based on the work by Beroza [1991], and we use a background stress orientation of $N6^\circ E$ [Amelung and King, 1997]. The Northridge earthquake is parameterized as a single plane based on the results of Dreger [1994] and Wald *et al.* [1996], and we use a principle stress direction of $N16^\circ E$ [Stein *et al.*, 1994]. For the Hector Mine earthquake we use a multiple slip patch file provided by Ross Stein (personal communication) based

on the results of Ji *et al.* [2000]. For each stress change calculation we resolve the stress onto optimally oriented fault planes; for the Loma Prieta earthquake we also resolve the stress change onto the plane of the Hayward fault, where a Loma Prieta induced stress shadow has been hypothesized [Reasenber and Simpson, 1997; Parsons *et al.*, 1999]. The stress changes are calculated in two dimensions, with 1 km grid spacing for the smaller Northridge and Loma Prieta earthquakes and 2 km grid spacing for the Landers and Hector Mine earthquakes. Thus an important assumption implicit in the calculations is that stress changes are uniform over the scale of 1 to 2 km.

[28] In order to get a range of possible stress change maps for the Landers earthquake we try frictional coefficients of 0.2, 0.4 and 0.8, and depths of 4, 7.5, and 12 km. We find that changes in the size of the stress shadow from small changes in friction and depth are not significant, and for the other earthquakes use only frictional coefficients of 0.4 and 0.8 and depths of 7.5 and 12 km. We truncate maximum positive stress changes at 30 bars, and negative stress change at -8 bars. The truncations are done to correct for unreasonably high stress changes that occur near modeled fault edges. The negative stresses are truncated more strongly than the positive stress changes because without such truncation the majority of the stress shadow signal comes from just a few grid cells with the highest stress changes. If these few stresses are in error, then we will erroneously assume a stronger stress shadow in the simulation. Since the purpose of our simulations is to find whether a reasonable stress shadow is observable with our method, being conservative requires testing whether the shadow factor can recover small stress shadows, not exceptionally large ones. Thus we eliminate these highly negative stresses in the simulations. We chose 8 bars for the cut off because this is the level where Toda *et al.* [1998] think that measurements are reasonable enough to compare static stress changes to seismicity rate changes. At the same time we allow the positive stresses to be as high as 30 bars because a strong aftershock signal also shrinks the visible stress shadow.

[29] To translate the calculated static stress changes into changes in earthquake rupture times, we need parameters for the rate and state friction equations. The form of the equations used, from Dieterich [1994], is given in Appendix A. We use a normal stress of 100 bars, an initial shear stress of 60 bars, a background stressing rate of 4.7×10^{-10} MPa s^{-1} , and A parameter values of 0.012, 0.008, and 0.005. These values of the A parameter cover the range considered reasonable based on laboratory experiments [Dieterich, 1994].

[30] Finally, our simulations require times and places of earthquakes occurring before the main shock and the locations and initial (e.g. what would have happened without the main shock) rupture times of earthquake sources that are affected by the main shock. We form these earthquake catalogs in several different ways. For the first way, which we term random catalog simulations, we assign the pre and postmain shock earthquakes randomly in time and space, using as guidelines the percentage of 1×1 km or 2×2 km bins (depending on the grid spacing of the respective stress change map) that are occupied by the actual earthquake catalog from 1 January 1984 through the date of the respective main shock. The temporal

Table 1. Seismicity Rates Measured in Data and Used in Simulations^a

Main Shock	Remain Shock Average	Random Catalog Simulation	Data-Based Simulation
Loma Prieta	3.04×10^{-5}	1.23×10^{-6}	9.8×10^{-6}
Landers	3.04×10^{-5}	5.74×10^{-6}	2.26×10^{-5}
Northridge	1.55×10^{-5}	1.05×10^{-6}	2.60×10^{-6}
Hector Mine	8.67×10^{-5}	6.50×10^{-6}	4.34×10^{-5}

^aMean rate of earthquakes measured from 1 January 1984, to the date of the main shock. For Loma Prieta, Landers, and Hector Mine earthquakes, $M \geq 2.3$, and for Northridge, $M \geq 2.0$. Rates are $\text{d}^{-1} \text{km}^{-2}$. Rates used for the random catalog simulations and rates used for the data-based simulations are meant to be instantaneous rates at the time of the main shock (as opposed to mean rates) and are chosen for the best match between the normalized shadow factor measured in simulations and data when no stress shadow is imposed.

earthquake rate used for these simulations is chosen such that the mean simulated shadow factor when stress changes are not imposed agrees as closely as possible with the mean shadow factor measured in the real control catalogs (Table 1). These best fit rates are typically lower than the mean premain shock catalog rates, most likely because the frequent sharp peaks in seismicity rate from various aftershock sequences causes the mean to be larger than the median.

[31] The advantage of the random catalog simulations is that the initial earthquake rate is the same for the premain shock and postmain shock periods. The disadvantage is that we cannot investigate the effects of realistic earthquake clustering in time and space. To address this, we also do what we term data-based simulations. For these simulations we use the actual earthquake catalog for the premain shock period; for the postmain shock period we assign initial earthquake times randomly but locate them within the same 1×1 or 2×2 km bins that contained premain shock earthquakes and distribute them proportionally in accordance with how many premain shock earthquakes were in

each bin. As before, we set the overall rate of these postmain shock earthquakes according to what provides the best agreement, in nonstressed simulations, with the stress shadow factor measured in the real control catalogs. We do one set of data-based simulations with the stress changes as calculated and another set with the stress changes on the map randomly rearranged (Figure 7b). In effect the randomized stress maps are a worse case scenario in which we assume that we have calculated the proper range of stress changes but completely mislocated them. Histograms of the time ratio distribution for data-based simulations of the Landers earthquake, compared to histograms of time ratios taken from the actual data, are given in Figure 6.

[32] For each simulation scenario we produce control catalogs by doing 100 simulations with no stress changes imposed. These control simulations provide the basis for measuring the normalized shadow factor. Results from both the random catalog simulations and data based simulations indicate that the majority of the time the normalized shadow factor is significant when a stress shadow is imposed. This

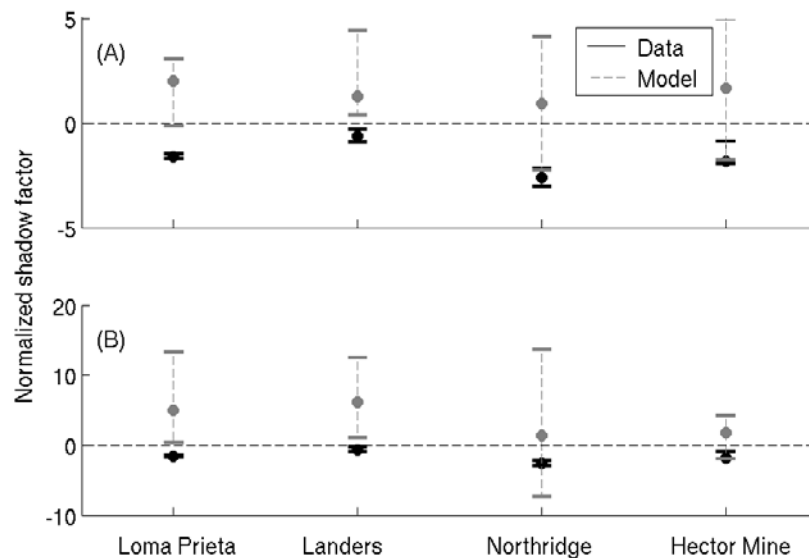


Figure 7. To test for whether or not there is a stress shadow, we compare the normalized shadow factors for the data and for simulations in which stress increases and shadows have been imposed. Black dots and 2σ confidence intervals give the measurements for the data; gray dots and error bars represent the simulations. The dot for each simulation is the mean value for the coefficient of friction 0.4, depth 7.5, and $A = 0.008$. The range of the error bars gives the most extreme values for all frictional coefficients, depths, and receiver fault orientations tried. (a) Data compared to the random earthquake simulations (B) Data compared to the data-based simulations done with randomized stress maps (which increase the error) (see text).

means that in general our test should be sufficiently sensitive to pick up stress shadows.

3.3. Results

[33] In the real data the normalized shadow factors for the four main shocks are less than zero (Figure 7), sometimes significantly so. This indicates that there is actually less seismicity rate decrease after the main shocks than at normal times in the catalog, probably in part a result of widespread aftershock activity. In contrast, for our simulations that contain both aftershocks and stress shadows the mean normalized shadow factor when we use average parameters (frictional coefficient 0.4, depth 7.5 km, $A = 0.008$) is larger than 2 (Figure 7). We find that two standard deviations corresponds closely to the 98% confidence level as determined by empirical cumulative distribution functions (CDFs). Thus normalized shadow factors over 2 may be considered to be significant.

[34] In Figure 7, error bars on the normalized shadow factors for the simulations, set at 2 standard deviations, are based on the largest standard deviation obtained for any combination of friction, depth, and A value parameters in sets of 100 trials done with each parameter set. In the case of the random catalog simulations the locations of the earthquakes on the stress map is also moved around for each trial; for the data-based simulations the error bars include different randomized stress maps. All of these factors make the simulation error bars quite wide. Nonetheless, for the Landers and Loma Prieta earthquakes there is no overlap between the error bars for the simulations and the data. The normalized shadow factor for the data is significantly lower than for the simulations, indicating a lack of stress shadow. For the Northridge and Hector Mine earthquakes the errors on the simulations are especially large, and there is overlap between the error bars for the data and simulations. This prevents us from strongly ruling out the possibility that stress shadows exist for these two earthquakes that our metric has simply failed to pick up. Yet the fact that as for the Landers and Loma Prieta earthquakes, the normalized shadow factors for Hector Mine and Northridge are both less than zero, suggests that stress shadows were not produced by these two earthquakes either.

[35] In summary, we find that for the data the normalized shadow factors are less than zero, indicating that there is actually less rate decrease right after our main shocks than there is at random times in the catalog. In contrast when we simulate stress shadows we get significantly positive normalized shadow factors in most cases. This difference between the normalized shadow factors for the stress shadow simulations and actual data indicates that stress shadows are absent from the data with 98% confidence for the Landers and Loma Prieta main shocks. For the Hector Mine main shock the upper 2% of the shadow factor distribution (the distribution above 2σ) intersects the shadow factor distribution of the simulations at -1.35σ , indicating a probability of at least 91% that the main shock did not produce a stress shadow (using a one tail normal distribution). For the Northridge main shock the upper 2% of the shadow factor probability distribution intersects the shadow factor distribution for the data-based simulations (which have larger error than the random catalog simulations) at 1.02σ , indicating that

we can be at least 84% confident that a stress shadow was not produced.

4. The 1906 San Francisco Earthquake

[36] The primary advantage of studying the four earthquakes that we have just investigated is that they are relatively recent earthquakes, occurring within instrumental catalogs. They are not, however, the largest earthquakes that California has ever experienced. Traditionally, the much larger 1906 San Francisco earthquake has been seen as one of the strongest and definitive examples of stress shadowing [Willis, 1924; Ellsworth *et al.*, 1981; Bufe and Varnes, 1993; Jaume and Sykes, 1996; Harris and Simpson, 1998; Bakun, 1999; Stein, 1999]. The primary argument for the shadow is that there were more earthquakes in the San Francisco Bay area in the 50 to 75 years before 1906 than over the same period of time afterward. The catalog compiled by Bakun [1999], places the earthquake ratio for the 50 years before versus the 50 years after 1906, for $M \geq 5.5$ earthquakes, at about 4.5.

[37] How sure can we be that the 1906 earthquake actually did produce a stress shadow in the San Francisco Bay Area? One of the first problems to address is the accuracy of the measured seismicity rate ratio, particularly since a large part of the catalog is historical. In particular historical data has very large location errors, in this case on the order of 50 to 100 km. In addition, locations are biased by population centers. Another issue is that a high cutoff magnitude of 5.5 must be used to ensure completeness [Bakun, 1999]. This limits the total number of earthquakes that can be counted from 50 years before through 50 years after 1906 to 45 (37 before the main shock and 8 afterward according to the combined catalogs of Bakun [1999] and Meltzner and Wald [2003]). According to Fisher's test for ratios [Fisher and Yates, 1964] this means that the actual seismicity rate ratio, within 95% confidence bounds, may have been between 2.1 and 11.5. There also tends to be higher magnitude uncertainties for older earthquakes, and because most earthquakes are small, larger magnitude uncertainties lead to higher probabilities that an earthquake had a smaller magnitude than assigned. The propensity for earthquakes to be small is quantified by the Gutenberg-Richter magnitude-frequency relationship [Ishimoto and Iida, 1939; Gutenberg and Richter, 1944]. Performing Monte Carlo simulations in which we combine the magnitude errors given in Bakun [1999], the Gutenberg-Richter distribution (with a b value of 1.0) and Fisher's test for ratios, we get 95% confidence limits between 1.7 and 11.3 for the ratio of seismicity in the 50 years before versus 50 years after 1906. We thus conclude that there were probably fewer earthquakes in the 50 years after 1906 than in the 50 years before, but the exact ratio is uncertain. We next look at the timing and location of this decrease in seismicity.

[38] In terms of timing, there was not a sudden seismic quiescence in the San Francisco Bay area immediately following the 1906 earthquake as would have been expected in the case of a classical stress shadow. According to the Townley-Allen catalog of felt seismicity [Townley and Allen, 1939], an average of about 4 earthquakes per year were felt in Berkeley between 1895 and 1905; in 1906, 96

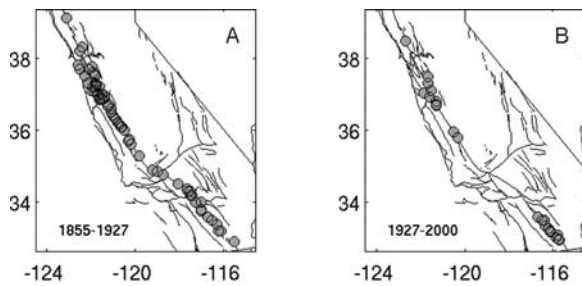


Figure 8. Large earthquakes along the entire San Andreas fault system have been less common in the last 75 years. (a) $M > 5.5$ earthquakes in from 1855 to 1927 within 15 km of the San Andreas, San Jacinto, and Hayward faults. (b) $M > 5.5$ earthquakes 1927–2000. This suggests that seismicity rate decreases in the Bay Area might have been caused by a regional rather than a local effect, e.g., the decay of aftershocks of the 1857 Fort Tejon earthquake rather than a 1906 induced stress shadow. Data are from California Geological Survey catalog, with historical earthquakes based on the work by *Topozada et al.* [2002].

earthquakes were felt [Lawson, 1908]. Even if we restrict ourselves to the largest earthquakes, quiescence did not set in until about 1927 [Bufe and Varnes, 1993; Jaume and Sykes, 1996]. A M 5.6 earthquake occurred in May 1906 around San Juan Batista [Meltzner and Wald, 2003], a M 6.2 occurred on the Calaveras fault in 1911, and $M > 5.5$ earthquakes occurred near Monterey in 1910 and 1926 [Bakun, 1999]. The lack of an immediate quiescence, and in particular the tremendous spike of seismicity in 1906, indicates with certainty that the entire Bay Area was not stress shadowed by the 1906 earthquake. To the contrary, at least part of the area clearly experienced stress triggering. This observation does not allow us to rule out the possibility of a mix of stress triggering and stress shadowing, however. According to the rate and state friction model [Dieterich, 1994] because the initial rate increase in triggered areas is much sharper than the initial rate decrease in shadowed areas a mix of triggering and shadowing is expected to result in early aftershocks followed by a longer-term quiescence.

[39] The strongest evidence that the long-term seismicity rate decrease in the San Francisco Bay Area probably does not indicate even a partial stress shadow, however, is that the average rate of recorded $M > 5.5$ earthquakes also decreased to the south of the 1906 rupture [Bakun, 2000; Topozada et al., 2002]. This is contrary to the static stress triggering model, which would predict a pure stress increase off the fault tip [Harris and Simpson, 1998]. We took the California Geological Survey catalog from 1855–2000 (which combines large historic and instrumental earthquakes) and compared the second half of the catalog (1927–2000) to the first half (1855–1927). (For reference, the instrumental earthquake catalog starts in 1932). We found that a decrease in $M \geq 5.5$ seismicity can in fact be found along the entire extent of the fault system, from the Bay Area through southern California (Figure 8).

[40] This system-wide decrease in the seismicity rate strongly suggests that the cause of the seismicity decrease was not a 1906 induced stress shadow as defined here.

One possibility is a systematic offset of the historical catalog in both regions with respect to the instrumental one, in the form of either a magnitude offset or a tendency to shift earthquakes toward the San Andreas fault. Another possibility is the decay of aftershocks of the larger 1857 Fort Tejon earthquake. The 1857 earthquake involved a long section of the San Andreas fault and was strongly felt in San Francisco [Wood, 1955]. Because most earthquakes trigger most of their aftershocks on or near their rupture plane and off the edge of the rupture, the 1857 earthquake would have been expected to trigger a lot of earthquakes along the San Andreas fault system in the second half of nineteenth century, the frequency of which would decay with time.

[41] The hypothesis that the Bay Area rate change can be explained by a decay of 1857 aftershocks would be supported by reports of local aftershocks in San Francisco immediately after the 1857 main shock. Unfortunately, a general survey of San Francisco newspapers indicates that they were notoriously bad at reporting aftershocks; the main newsworthy items were the main shock itself and the damage it caused. The *Daily Alta* did, however, publish the following account on 13 January 1857, five days after the main shock: “More Earthquakes – We have had several persons assert that they felt the shock of an earthquake last evening around 11:00. Old Mother Earth appears to be in a very shaky sense of humor lately.” The Townley-Allen catalog [Townley and Allen, 1939] does not list aftershocks of the 1857 earthquake for any location between the main shock date of 9 January and 17 January, suggesting the confusion and incompleteness of reports that often accompanies the initial aftermath of a large earthquake. Between 17 and 22 January, however, separate earthquakes are reported not only in Los Angeles and Fort Tejon but also in the northern California cities of Martinez, Benecia, Santa Cruz, San Juan Batista, San Benito, and Mariposa, suggesting 1857 aftershock activity in the Bay Area, both to the north and south of San Francisco. Overall, the catalog specifically mentions San Francisco in 19 earthquake entries in 1857, in comparison to 14 entries in 1856, 7 entries in 1858, 14 in 1859, and 10 in 1860. In addition, if we assume that the 1857 aftershocks followed a simple Omori’s law $1/\text{time}$ decay rate, then we would predict about 5.5 times more earthquakes from 1858 to 1906 than from 1907 to 1955; in comparison the ratio given over these time periods in the combined catalogs of Bakun [1999] and Meltzner and Wald [2003] is 5.6. We would, however, expect more $M \geq 5.5$ earthquakes in 1857 itself, which are not listed in the Bakun [1999] catalog. It is possible that several of the many Bay Area 1857 earthquakes were relatively large but were not fully covered in the newspapers due to aftershock fatigue.

[42] In summary we find that statistically there does appear to have been a lower seismicity rate in the first half of the twentieth century than in the last half of the nineteenth century in the San Francisco Bay Area. Right after the 1906 main shock, however, there was a sharp seismicity rate increase, not decrease, indicating at least part of the Bay Area could not have been in a stress shadow. We also find that the recorded long-term rate change is not confined to the Bay Area; it can also be seen all along the southern extension of the San Andreas fault system. This

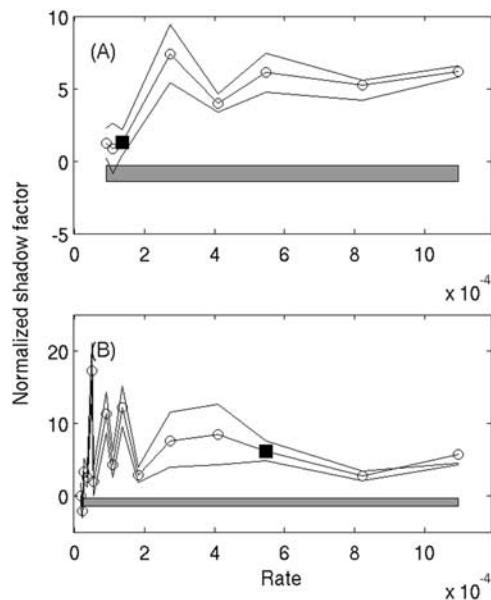


Figure 9. Resolvability of a stress shadow is dependent on the preexisting earthquake rate. For the Landers earthquake we plot the normalized shadow factor of simulated catalogs with stress shadows imposed on them, for different initial seismicity rates. We do 100 simulations at each rate; the central line with the circles represents the mean result, and the outer black lines are plotted at the upper and lower 2σ . The black square is plotted at the initial seismicity rate that best fits the catalog data. The gray area represents the normalized shadow factor $\pm 2\sigma$ for the actual data. When the solid line for the bottom limit of the 98% confidence interval intersects the gray area we can no longer resolve at high confidence whether or not the data contains a stress shadow. (a) Random earthquake simulations. (b) Data-based simulations with a randomized stress map.

indicates that the rate decrease was probably not caused by even a partial stress shadow of the earthquake, which would not have been expected to extend off the southern tip of the rupture. Instead, the observation can most likely be explained either by inconsistencies between the historical and instrumental catalogs or the decay of aftershocks of the Great 1857 Fort Tejon San Andreas fault earthquake.

5. Discussion

[43] Because of its size and its strong traditional association with a stress shadow, the 1906 San Francisco earthquake is important for us to investigate. However, because of unavoidable limitations on historical data our results from the modern, instrumented catalog are the strongest part of our analysis. For the four modern earthquakes that we have studied we find that we can be confident that the seismicity rate decreases measured by the normalized shadow factor at the time of our main shocks are less than at other times in the catalog. This suggests strong aftershock activity and the lack of a stress shadow. However, have we adequately dealt with the probability that the null hypothesis has been accepted incorrectly because our test is not sensitive enough? The concern is that our type II error analysis is

strongly simulation based. What if our simulations are not realistic enough? In particular, as mentioned above, our stress shadow measurement is sensitive to the preexisting seismicity rate, and to the initial seismicity rate that we assign to the future earthquake sources before they are stressed or shadowed. What if we have estimated the initial rate incorrectly? We do an additional set of simulations in which we gradually decrease the earthquake rate to find at what rate the normalized shadow factor calculated for the simulation is statistically indistinguishable from the factor calculated from the data (Figure 9 and Table 2). In most cases this point is either reached well below the rate that is judged to be the best fit for the data or the point simply cannot be reached, even when there are no catalog earthquakes at all after the main shock.

[44] In addition to the earthquake rates there are many other free variables in the simulations. We have tried a wide gamut of coefficients of friction, depth of calculation, and the rate and state friction A parameter, but have not tried every single combination of initial stresses and background stressing rates, have not considered a wide variation of aftershock focal mechanisms, have not tried every main shock slip inversion solution. We have not put in a nonhomogeneous half-space, or secondary aftershock triggering, both of which can be quite important. It is possible that if we tried more and more variations, we would find some scenarios in which we could not see the stress shadow with our test. It is impossible to prove a negative. All we can say is that if stress shadows roughly have the same strength and extent as the ones that we have modeled, using the standard static stress triggering aftershock theory with standard parameters, then they do not exist after the Loma Prieta, Landers, Northridge, or Hector Mine earthquakes, which are among the best recorded earthquakes available in California.

[45] Another issue is that for the purposes of this paper we have looked only for the type of instant stress shadow that would be produced if a strong majority of aftershocks are triggered via static stress changes and rate and state friction. Hybrid models, such as the one proposed by *Voisin et al.* [2004], have dynamic triggering for the early, most active part of the aftershock sequence, combined with static stress triggering later on. Because the stress shadow in the hybrid model would be delayed, it is likely that we would not detect it with our test. Most aftershocks

Table 2. Lowest Seismicity Rates for Which a Stress Shadow Would Be Resolvable^a

Main Shock	Random Catalog Simulation	Data-Based Simulation
Loma Prieta	$<5.13 \times 10^{-7}$	$<3.92 \times 10^{-7}$
Landers	3.83×10^{-6}	9.0×10^{-7}

^aThe seismicity rate at which there would be overlap between the 98% confidence bars for the simulations and the data is given. Rates are given in earthquakes $\text{d}^{-1} \text{km}^{-2}$. See Table 1 to compare to the best fit instantaneous seismicity rates and the average premain shock catalog seismicity rates. Separate values are given for the random catalog simulations and the data-based simulations (done with a randomized stress map). The Loma Prieta values are given as maximums because of the lack of a sufficient number of earthquakes at rates lower than this prevents a continuation of simulations. The Northridge and Hector Mine earthquakes are not listed here because there is already some overlap of 98% confidence error bars at the best fit seismicity rate (Figure 7).

are triggered by dynamic stress changes in the hybrid model, however.

6. Conclusions

[46] We have devised a time ratio metric to test whether stress shadows were created after several large main shocks in California. The amount of seismicity rate decrease detected by this metric after the Loma Prieta, Landers, Northridge, and Hector Mine earthquakes was less than the amount detected after random points of time in the catalog. Simulations suggest that this result would have been unlikely if the main shocks imposed stress shadows, suggesting that stress shadows are absent after these four main shocks. Because of lack of adequate data we cannot use the time ratio to test for a stress shadow after the 1906 San Francisco earthquake, one of the earthquakes for which the production of a stress shadow has long been hypothesized. We find, however, that the seismicity rate decrease in the first half of the twentieth century in the Bay Area, often attributed to a 1906 stress shadow, is mirrored by decreases all along the San Andreas fault system. This suggests nonstress shadow reasons for the rate decrease, such as the decay of aftershocks of the 1857 Fort Tejon earthquake.

[47] Our results suggest that there is little strong evidence that stress shadows exist. This implies that aftershock triggering is not driven entirely by static stress changes. Instead, the result suggests that aftershocks are either triggered entirely by dynamic stress change or by a mix of dynamic and static stress changes. It is true that dynamic stresses are only applied temporarily while static stress changes are permanently applied to the fault plane. However, anyone who has been close to a powerful earthquake can attest that temporary shaking can have permanent damaging effects. Work has been done to demonstrate the plausibility of dynamic triggering leading to aftershock decay in accordance with Omori's law [Parsons, 2005], and more work is in progress. The challenge that lies ahead is to further develop and work on these models to see if one can be found that meets with general acceptance in the seismological community.

Appendix A: Rate and State Friction Equations Used in Simulations

[48] For our stress shadow simulations we translate calculated static stress changes into changes in earthquake rupture times using the rate and state friction equations (A13) and (A17) of [Dieterich, 1994]. The specific algorithm for a single earthquake fault is as follows:

[49] 1. An initial earthquake rupture time, t_1 , is assigned to the fault.

[50] 2. The initial rupture time is translated into an initial fault slipping velocity v_0 :

$$v_0 = c / \left(e^{t_1/b} - 1 \right) \quad (\text{A1})$$

where $c = \dot{\tau}/H\sigma$, $b = A\sigma/\dot{\tau}$ and $H = 0.08/\sigma$, $\dot{\tau}$ is the stressing rate, σ is the normal stress, and A is a parameter that is varied between 0.005 and 0.012 for different simulations.

[51] 3. A stress change is applied and translated into a new slipping velocity, v_2 ,

$$v_2 = v_0 e^{(CF - CF_0)/A\sigma_0} \quad (\text{A2})$$

where CF indicates Coulomb stress, a subscript of 0 denotes initial stresses before the occurrence of the main shock, and $CF = \tau + \mu\sigma$ where τ is shear stress, μ is the coefficient of friction, and σ is normal stress. This expression is a simplification of equation (A17) of Dieterich [1994], which provides for complex changes in the fault state as a result of change in the normal stress. In the absence of unusually strong sensitivity of the fault state to changes in normal stress, this simplification provides a solution that is on the same order of magnitude as the full equation.

[52] 4. Finally, the new slipping velocity is translated back into a new time to rupture, t_2

$$t_2 = b \times \ln((c/v_2) + 1) \quad (\text{A3})$$

[53] **Acknowledgments.** We would like to gratefully acknowledge the many people who have provided helpful comments, thorough reviews, and analysis during the different stages of this work. These include Rachel Abercrombie, Ruth Harris, Paul Reasenber, Bob Simpson, David Marsan, Andy Freed, Ross Stein, Jeanne Hardebeck, Agnes Helmstetter, Jim Dieterich, Ellen Mallman, Alan Felzer, Mike Harrington, and a number of others. We are also very grateful to Associate Editor Joan Gomberg and careful reviews by Stefan Wiemer and an anonymous reviewer. Earthquake catalog data were made available by the Council of the National Seismic System, the Southern California Earthquake Data Center, the California Institute of Technology, the Northern California Earthquake Data Center, the Berkeley Seismological Laboratory, and the Northern California Seismic Network. Support for this work was provided by the National Science Foundation grant EAR 0409731. Support was also provided by the Southern California Earthquake Center. SCEC is funded by NSF Cooperative Agreement EAR-0106924 and USGS Cooperative Agreement 02HQAG0008. This is SCEC contribution 869.

References

- Amelung, F., and G. King (1997), Large-scale tectonic deformation inferred from small earthquakes, *Nature*, 386, 702–705.
- Bakun, W. H. (1999), Seismic activity of the San Francisco Bay region, *Bull. Seismol. Soc. Am.*, 89, 764–784.
- Bakun, W. H. (2000), Seismicity of California's north coast, *Bull. Seismol. Soc. Am.*, 90, 797–812.
- Beroza, G. C. (1991), Near-source modeling of the Loma Prieta earthquake: Evidence for heterogeneous slip and implications for earthquake hazard, *Bull. Seismol. Soc. Am.*, 81, 1603–1621.
- Bufe, C. G., and D. J. Varnes (1993), Predictive modeling of the seismic cycle of the greater San Francisco Bay region, *J. Geophys. Res.*, 98, 9871–9883.
- Davies, J. N., L. Sykes, L. House, and K. Jacob (1981), Shumagin seismic gap, Alaskan Peninsula: History of great earthquakes, tectonic setting, and evidence for high seismic potential, *J. Geophys. Res.*, 86, 3821–3855.
- Dieterich, J. A. (1994), Constitutive law for the rate of earthquake production and its application to earthquake clustering, *J. Geophys. Res.*, 99, 2601–2618.
- Dreger, D. S. (1994), Empirical Green's function study of the January 19, 1994, Northridge, California earthquake, *Geophys. Res. Lett.*, 21, 2633–2636.
- Ellsworth, W. L., A. G. Lindh, W. H. Prescott, and D. G. Herd (1981), The 1906 San Francisco earthquake and the seismic cycle, in *Earthquake Prediction: An International Review*, Maurice Ewing Ser., vol. 4, edited by D. W. Simpson and P. G. Richards, pp. 126–140, AGU, Washington, D. C.
- Felzer, K. R., R. E. Abercrombie, and Göran Ekström (2003), Secondary aftershocks and their importance for aftershock prediction, *Bull. Seismol. Soc. Am.*, 93, 1433–1448.
- Fisher, R. A., and F. Yates (1964), *Statistical Tables for Biological, Agricultural, and Medical Research*, Oliver and Boyd, White Plains, N. Y.
- Geschwind, C.-H. (2001), *California Earthquakes: Science, Risk, and the Politics of Hazard Mitigation*, 337 pp., John Hopkins Univ. Press, Baltimore, Md.

- Gomberg, J., P. Bodin, and P. A. Reasenberg (2003), Observing earthquakes triggered in the near field by dynamic deformations, *Bull. Seismol. Soc. Am.*, *93*, 118–138.
- Gutenberg, B., and C. F. Richter (1944), Frequency of earthquakes in California, *Bull. Seismol. Soc. Am.*, *4*, 185–188.
- Hardebeck, J. L., J. J. Nazareth, and E. Hauksson (1998), The static stress change triggering model: Constraints from two southern California aftershock sequences, *J. Geophys. Res.*, *103*, 24,427–24,437.
- Harris, R. A., and R. W. Simpson (1998), Suppression of large earthquakes by stress shadows: A comparison of Coulomb and rate-and-state failure, *J. Geophys. Res.*, *103*, 24,439–24,451.
- Helmstetter, A., and D. Sornette (2002), Subcritical and supercritical regimes in epidemic models of earthquake aftershocks, *J. Geophys. Res.*, *107*(B10), 2237, doi:10.1029/2001JB001580.
- Hill, D. P., et al. (1993), Seismicity remotely triggered by the magnitude 7.3 Landers, California, earthquake, *Science*, *260*, 1617–1623.
- Ishimoto, M., and K. Iida (1939), Observations of earthquakes registered with the microseismograph constructed recently, *Bull. Earthquake Res. Inst. Univ. Tokyo*, *17*, 443–478.
- Jaume, S. C., and L. R. Sykes (1996), Evolution of moderate seismicity in the San Francisco Bay region, 1850 to 1993: Seismicity changes related to the occurrence of large and great earthquakes, *J. Geophys. Res.*, *101*, 765–789.
- Ji, C., D. J. Wald, and D. V. Helmlinger (2000), Slip history of the 1999 Hector Mine, California earthquake, *Seismol. Res. Lett.*, *71*, 224.
- Kagan, Y. Y., and D. D. Jackson (1991), Seismic gap hypothesis: Ten years after, *J. Geophys. Res.*, *96*, 21,419–21,431.
- Kilb, D., J. Gomberg, and P. Bodin (2002), Aftershock triggering by complete Coulomb stress changes, *J. Geophys. Res.*, *107*(B4), 2060, doi:10.1029/2001JB000202.
- King, G. C., R. S. Stein, and J. Lin (1994), Static stress change and the triggering of earthquakes, *Bull. Seismol. Soc. Am.*, *84*, 935–953.
- Lawson, A. C. (1908), *The California Earthquake of April 18, 1906: Report of the State Earthquake Investigation Commission*, vol. 1, 451 pp., Carnegie Inst. of Washington, Washington, D. C.
- Marone, C. (2000), Earthquake science: Shaking faults loose, *Nature*, *408*, 533–535.
- Marsan, D. (2003), Triggering of seismicity at short timescales following Californian earthquakes, *J. Geophys. Res.*, *108*(B5), 2266, doi:10.1029/2002JB001946.
- Meltzner, A. J., and D. J. Wald (2003), Aftershocks and triggered events of the great 1906 California earthquake, *Bull. Seismol. Soc. Am.*, *93*, 2160–2186.
- Ogata, Y., L. M. Jones, and S. Toda (2003), When and where the aftershock activity was depressed: Contrasting decay patterns of the proximate large earthquakes in southern California, *J. Geophys. Res.*, *108*(B6), 2318, doi:10.1029/2002JB002009.
- Omori, F. (1907), Preliminary note on the course of the California earthquake of 1906, in *The California Earthquake of 1906*, edited by D. S. Jordan, pp. 281–318, A. M. Robertson, San Francisco, Calif.
- Parsons, T. (2005), A hypothesis for delayed dynamic earthquake triggering, *Geophys. Res. Lett.*, *32*, L04302, doi:10.1029/2004GL021811.
- Parsons, T., R. S. Stein, R. W. Simpson, and P. A. Reasenberg (1999), Stress sensitivity of fault seismicity: A comparison between limited-offset oblique and major strike-slip faults, *J. Geophys. Res.*, *104*, 20,183–20,202.
- Reasenberg, P. A. (1985), Second-order moment of central California seismicity, *J. Geophys. Res.*, *90*, 5479–5495.
- Reasenberg, P. A., and R. W. Simpson (1992), Response of regional seismicity to the static stress change produced by the Loma Prieta earthquake, *Science*, *255*, 1687–1690.
- Reasenberg, P. A., and R. W. Simpson (1997), Response of regional seismicity to the static stress change produced by the Loma Prieta earthquake, in *The Loma Prieta Earthquake of October 17, 1989 Aftershocks and Postseismic Effects*, edited by P. A. Reasenberg, *U.S. Geol. Surv. Prof. Pap.*, *1550*, D49–D71.
- Reid, H. F. (1910), The California earthquake of April 18, 1906: Report of the State Earthquake Investigation Commission, vol. 2, 32 pp., Carnegie Inst. of Washington, Washington, D. C.
- Simpson, R. W., and P. Reasenberg (1994), Earthquake-induced static-stress changes on central California faults, in *The Loma Prieta Earthquake of October 17, 1989 Aftershocks and Postseismic Effects*, edited by P. A. Reasenberg, *U.S. Geol. Surv. Prof. Pap.*, *1550*, F55–F89.
- Sornette, A., and D. Sornette (1999), Renormalization of earthquake aftershocks, *Geophys. Res. Lett.*, *26*, 1981–1984.
- Stein, R. S. (1999), The role of stress transfer in earthquake occurrence, *Nature*, *402*, 605–609.
- Stein, R. S. (2003), Earthquake conversations, *Sci. Am.*, *288*, 72–79.
- Stein, R. S., G. C. King, and J. Lin (1994), Stress triggering of the 1994 $m = 6.7$ Northridge, California, earthquake by its predecessors, *Science*, *265*, 1432–1435.
- Toda, S., and R. S. Stein (2002), Response of the San Andreas fault to the 1983 Coalinga-Nuñez earthquakes: An application of interaction-based probabilities for Parkfield, *J. Geophys. Res.*, *107*(B6), 2126, doi:10.1029/2001JB000172.
- Toda, S., and R. Stein (2003), Toggling of seismicity by the 1997 Kagoshima earthquake couplet: A demonstration of time-dependent stress transfer, *J. Geophys. Res.*, *108*(B12), 2567, doi:10.1029/2003JB002527.
- Toda, S., R. S. Stein, P. A. Reasenberg, J. H. Dieterich, and A. Yoshida (1998), Stress transfer by the $M_W = 6.9$ Kobe, Japan earthquake: Effect on aftershocks and future earthquake probabilities, *J. Geophys. Res.*, *103*, 24,543–24,565.
- Topozada, T. R., D. M. Branum, M. S. Reichle, and C. L. Hallstrom (2002), San Andreas fault zone, California: $m \geq 5.5$ earthquake history, *Bull. Seismol. Soc. Am.*, *92*, 2555–2601.
- Townley, S. D., and M. W. Allen (1939), Descriptive catalog of earthquakes of the Pacific coast of the United States: 1769 to 1928, *Bull. Seismol. Soc. Am.*, *29*, 1–297.
- Voisin, C., F. Cotton, and S. Di Carli (2004), A unified model for dynamic and static stress triggering of aftershocks, antishocks, remote seismicity, creep events, and multisegmented rupture, *J. Geophys. Res.*, *109*, B06304, doi:10.1029/2003JB002886.
- Wald, D. J., and T. H. Heaton (1994), Spatial and temporal distribution of slip for the 1992 Landers, California, earthquake, *Bull. Seismol. Soc. Am.*, *84*, 668–691.
- Wald, D. J., T. H. Heaton, and K. W. Hudnut (1996), The slip history of the 1994 Northridge, California, earthquake determined from strong-motion, teleseismic, GPS, and leveling data, *Bull. Seismol. Soc. Am.*, *86*, 49–70.
- Willis, B. (1924), Earthquake risk in California, *Bull. Seismol. Soc. Am.*, *14*, 9–25.
- Woessner, J., E. Hauksson, S. Wiemer, and S. Neukomm (2004), The 1997 Kagoshima (Japan) earthquake doublet: A quantitative analysis of aftershock rate changes, *Geophys. Res. Lett.*, *31*, L03605, doi:10.1029/2003GL018858.
- Wood, H. O. (1955), The 1857 earthquake in California, *Bull. Seismol. Soc. Am.*, *45*, 47–68.
- Wyss, M., and S. Wiemer (2000), Change in probability for earthquakes in southern California due to the Landers magnitude 7.3 earthquake, *Science*, *290*, 1334–1338.

E. E. Brodsky and K. R. Felzer, Department of Earth and Space Sciences, University of California, 3806 Geology Building, Box 951567, Los Angeles, CA 90095-1567, USA. (brodsky@ess.ucla.edu; kfelzer@moho.ess.ucla.edu)